Anal Bioanal Chem (2006) 385: 700–707
DOI 10.1007/s00216-006-0442-1

ORIGINAL PAPER

W. Lisowski · E. G. Keim · A. H. J. van den Berg · M. A. Smithers

# Structural and chemical characterisation of titanium deuteride films covered by nanoscale evaporated palladium layers

Received: 6 January 2006 / Revised: 27 February 2006 / Accepted: 17 March 2006 / Published online: 4 May 2006


**Abstract** Thin titanium deuteride ($TiD_y$) films, covered by an ultra-thin palladium layer, have been compared with the corresponding titanium and palladium films using a combination of scanning electron microscopy (SEM), transmission electron microscopy (TEM) and X-ray photoelectron spectroscopy (XPS). The $TiD_y$ layers were prepared under ultra-high vacuum (UHV) conditions by precisely controlled deuterium sorption at 298 K on a Ti film evaporated onto a Si(100) substrate. Both Ti and $TiD_y$ films were then covered in situ by a nanoscale Pd layer. It was found that a 10- to 12-nm-thick Pd layer protects the $TiD_y$ films efficiently against extensive air interaction. The morphology of both the surface and bulk Pd/$TiD_y$ (Ti) films have been observed using SEM and cross-sectional TEM analysis, respectively. A polycrystalline bulk morphology in both Ti and $TiD_y$ films accompanied by a fine-grained Pd surface was observed. High-magnification cross-sectional TEM images reveal the $TiD_y$ film to be plastically deformed leading to an increase in the roughness of the top Pd layer. Complex structures, including Moiré patterns, have been identified within the Pd/$TiD_y$ interface. The chemical nature of this interface has been analysed after partial sputtering of the Pd top layer using XPS. Besides $TiD_y$ and Pd, TiO and PdO were found to be the main chemical species in the interface region of the Pd/$TiH_y$ film. The XPS valence-band spectra of the Pd/$TiD_y$ interface reveal electronic features characteristic of a Pd–Ti bimetallic structure.

**Keywords** Titanium deuteride · SEM · TEM · XPS

W. Lisowski (✉)
Institute of Physical Chemistry,
Polish Academy of Sciences,
Kasprzaka 44/52,
01-224 Warszawa, Poland
e-mail: wlis@ichf.edu.pl

E. G. Keim · A. H. J. van den Berg · M. A. Smithers
MESA Research Institute, Central Materials Analysis Laboratory, University of Twente,
P.O. Box 217, 7500 AE Enschede, The Netherlands
e-mail: e.g.keim@tnw.utwente.nl

## Introduction

Thin films of titanium hydride (deuteride) have a number of possible applications as hydrogen (deuterium) storage material in catalytic or energetic reactions [1–3]. Recently, titanium hydride layers grown epitaxially on the surface of titanium implants were found to be a promising candidate for biomedical applications, because the plastically deformed hydride layer was found to accommodate externally applied stresses without disturbing the Ti body structure [4].

However, application of a $TiH_y$ film under atmospheric pressure, in spite of its rather high stability [2, 5, 6], leads to a partial decomposition of $TiH_y$ due to titanium oxide formation at the surface and subsurface regions and also to extensive penetration of oxygen into the bulk of the $TiH_y$ film [7]. To prevent air interaction with the titanium material, both titanium and titanium alloys were precovered with Pd protective layers [8] and subsequently used for titanium hydride formation under intensive hydrogen (deuterium) treatment at elevated temperatures [9]. The influence of a palladium coating on the adsorption properties of TiFe monocrystals has also been studied theoretically [10, 11].

In the present work we covered the titanium deuteride film, just after its formation at room temperature, by in situ evaporation of an ultra-thin Pd layer. In a similar way titanium hydride films were covered by a protective film using thin, post-evaporation of Au [12]. A combination of scanning electron microscopy (SEM), transmission electron microscopy (TEM) and X-ray photoelectron spectroscopy (XPS) allowed us to characterize the surface and bulk structure of Pd-protected titanium deuteride films, to identify the Pd/$TiD_y$ interface layer and to study both its

crystallographic structure and the chemical nature of the compounds forming the Pd/$TiD_y$ interface region.

## Experimental

Ti films were deposited onto a Si(100) substrate within a glass ultra-high vacuum (UHV) system [13], at a pressure $\leq 1\times10^{-7}$ Pa, by evaporation of a fine wire (Johnson-Matthey grade I) wound around a tungsten heater. During deposition of the films, the Si substrate was maintained at 273 K. The films were annealed for 60 min at 650 K.

The titanium deuteride ($TiD_y$) films were obtained in situ due to interaction of thin Ti films with spectroscopically pure deuterium additionally purified by diffusion through a palladium thimble. Deuterium was introduced in successive, calibrated doses at 298 K until an equilibrium pressure of 1 Pa was reached. Following this volumetrically controlled adsorption procedure, $TiD_y$ films were routinely obtained with $y \approx 2$ [14]. The chemical nature of the titanium hydride formed in the same experimental way was confirmed previously using SIMS analysis [12]. Both the Ti film and the Ti film which was exposed to deuterium were then covered in situ by a 6- to 20-nm-thick Pd layer evaporated from a fine Pd wire wound around a tungsten heater. Morphological and chemical examination of the Pd/Ti and Pd/$TiD_y$ films was performed ex situ in separate analytical systems.

SEM (LEO Gemini 1550 FEG SEM) was carried out to study the surface morphology of the films. Cross-sectional TEM analysis (Philips CM30 Twin (S)TEM), on the other hand, was performed to obtain information regarding the bulk structure of corresponding films and to reveal the nanostructures formed at the Pd/$TiD_y$ interface. Selected area diffraction (SAD) analysis allowed the crystal phases in the bulk of Pd/$TiD_y$ film to be identified. The TEM specimens of the Pd/$TiD_y$ films were prepared in cross-section according to a method described in [15].

XPS analyses were carried out in a PHI Quantera scanning X-ray microprobe. For calibration of the energy scale of the instrument, the work function of the spectrometer was determined by setting the binding energy (BE) values of Au $4f_{7/2}$, Ag $3d_{5/2}$ and Cu $2p_{3/2}$ for cleaned gold, silver and copper to 83.8, 368.2 and 932.8 eV [16–18], respectively, by using a Mg anode. The XPS spectra were recorded on "as received" specimens and after partially removing the top layer by means of argon ion sputtering with a 1.0-keV $Ar^+$ beam energy, a sputter area of 2×2 mm, a sputter rate of 2.9 nm $min^{-1}$, calibrated on a 100-nm-thick $SiO_2$ layer thermally grown on a Si substrate. The position of the C 1s peak relative to its normal position at BE=284.8 eV was used [17, 18] to correct the measured BE for electrostatic charging of all "as received" samples. The positions of Pd 3d5/2 and Pd 3p3/2 at 335.0 and 532.3 eV [19], respectively, were used additionally for the BE correction of both Ti and $TiD_y$ films covered with Pd after the argon ion etching treatment.

## Results and discussion

### SEM analysis

Figure 1 shows SEM images of Ti and $TiD_y$ film surfaces and the corresponding film surfaces covered by a 10- to 12-nm-thick Pd layer.The Ti film is characterised by a fine-grained (25–40 nm) surface morphology. Small grains are well separated but also aggregate into larger clusters (80–300 nm). This phenomenon was not observed on the Ti films evaporated at 78 K and annealed at 330 K [7]. Therefore, the aggregation of Ti grains can be ascribed in this case to a surface transformation induced by high-temperature (650 K) annealing of the Ti film.

A distinct change in the Ti film surface morphology has been observed after deuterium treatment leading to $TiD_y$ formation (Fig. 1b). Smaller grains are easily distinguish-

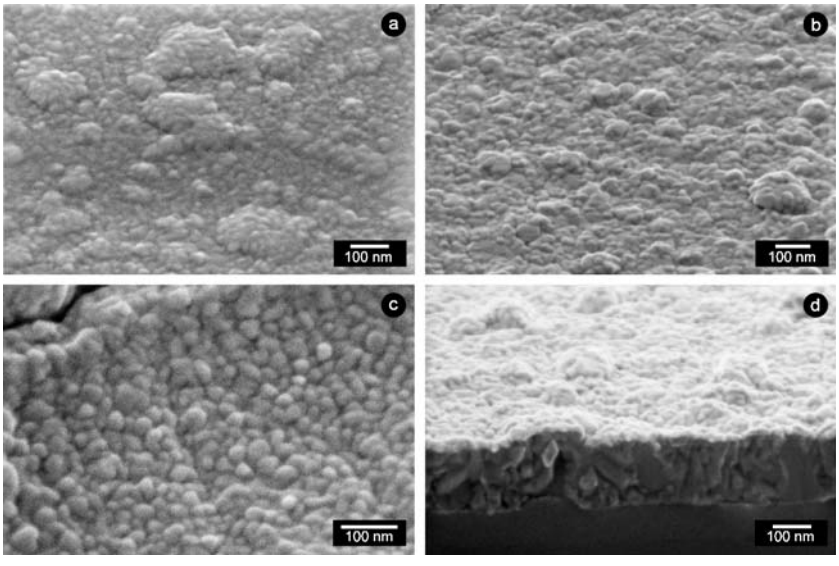


**Fig. 1** SEM images of **a** 100-nm-thick Ti film surface (surface view), **b** 100-nm-thick $TiD_y$ film surface (surface view), **c** 110-nm-thick Ti film covered by a 8- to 10-nm-thick Pd layer (surface view), **d** 170-nm-thick $TiD_y$ film covered by a 10- to 12-nm-thick Pd layer (cross-section view)

able and well separated, and extensive aggregation does not seem to occur.

A granular structure with a grain size of 20–40 nm can be observed on Ti and $TiD_y$ films covered by a 10- to 12-nm-thick Pd layer (Figs. 1c and d). Figure 1c shows a small number of micro-cracks in the top section of the Pd/Ti film. In the cross-sectional SEM image of the Pd/$TiD_y$ layer (Fig. 1d) it can be observed that the thin Pd layer is only weakly attached to the $TiD_y$ film and its surface grain corrugation is determined by the grain distribution within the bulk of the $TiD_y$ film.

## Cross-sectional TEM analysis

Figure 2 shows low-magnification TEM cross-sectional images of Ti and $TiD_y$ films, each covered by a 10- to 12-nm-thick Pd layer. The images reveal a polycrystalline structure in both films with polygonal and columnar grains. The Ti film, annealed at 650 K, is composed of randomly distributed and well distinguishable grains (Fig. 2a). Low-temperature sorption of deuterium leads to a coarsening of the surface and subsurface region of the Ti film, resulting in an increased roughness of the top Pd layer (Fig. 2b).

In order to obtain information on the microstructure of both $TiD_y$ and Ti films covered by a thin Pd layer, TEM selected area diffraction analyses were carried out. The SAD patterns were recorded on an area (diameter approximately 500 nm) including the cross-section planes of the Pd/$TiD_y$ and Pd/Ti film and part of the glue/vacuum layer. All SAD recordings show the diffraction spots to lie on a ring-like pattern. Figures 2c and d show a quarter-section representation of the SAD pattern from the Pd/Ti and Pd/$TiD_y$ film, respectively. From a direct measurement of the radius between the central spot and the diffraction spots lying on artificial concentric circles, shown in Figs. 2c and d as semitransparent grey circle sections drawn through the relevant diffraction spots, the Miller index planes could be determined. From the SAD patterns the complete set of crystallographic planes belonging to Pd and $TiD_2$ fcc structures, and Ti hcp structure could be identified. Our results show good agreement with those reported for Ti, $TiH_2$ and Pd [20, 21].

### *Structural variations at Pd/Ti and Pd/$TiD_y$ interfaces*

Figures 3, 4 and 5 show the high-magnification cross-sectional TEM lattice images of the Pd/Ti and Pd/$TiD_y$

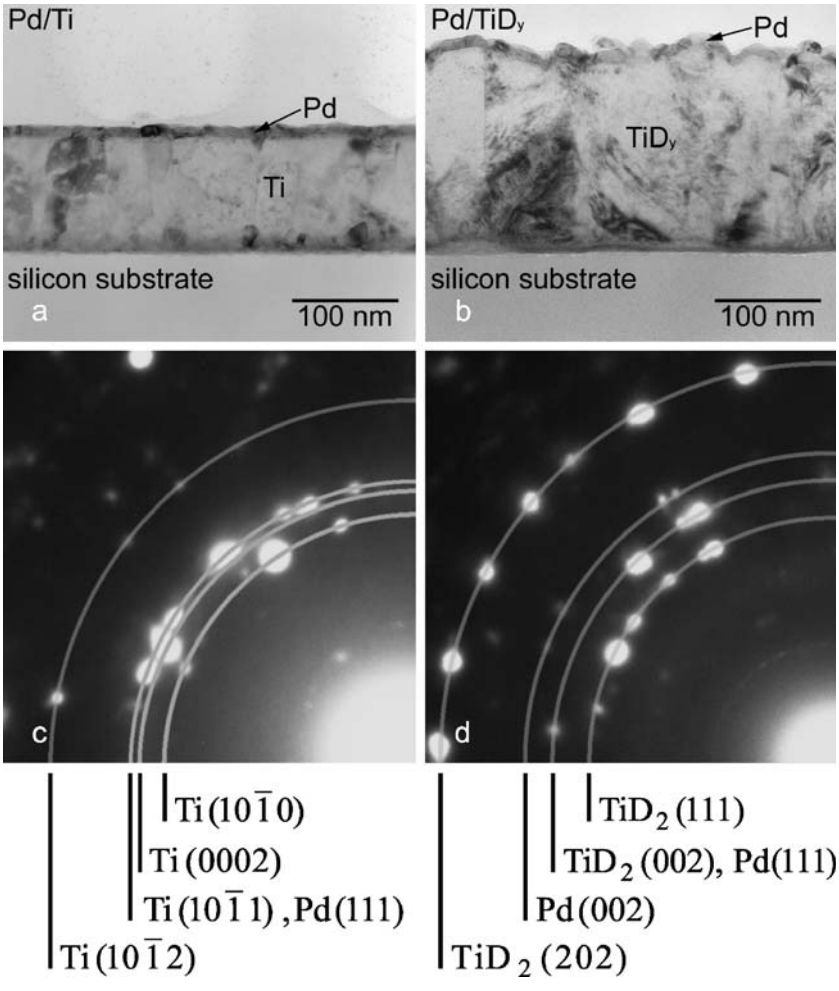


**Fig. 2** Low-magnification TEM cross-sectional bright-field images of the titanium (**a**) and the titanium deuteride (**b**) films covered by a 10- to 12-nm-thick palladium layer. The selected area diffraction (SAD) pattern recorded on the Pd/Ti and Pd/TiDy areas are shown in images **c** and **d**, respectively, in a quarter-section representation, together with the assignment of the most relevant low-index Miller planes of the diffraction spots

films, respectively. Careful analysis of these images allows one to identify the Pd/Ti and Pd/$TiD_y$ interface and characterize structures which are result of a crystallographic relationship between adjacent grains of Pd layer, and between these grains and the Ti and $TiD_y$ substrate.

Figure 3a shows a clearly distinguishable smooth, 6- to 8-nm-thick Pd top layer covering the Ti film. Figure 3b, an area zoomed-in from within the square box in Fig. 3a, reveals the Pd/Ti interface formed by $Ti_{(10\bar{1}1)}$ hcp and Pd (111) fcc structures. The interplanar distances of these structures as determined from the lattice fringes are very similar (0.224±0.004 [20, 21]), therefore suggesting a structural relationship between the Ti substrate and the Pd grains. The structural relationship also manifests itself by adjacent diffraction spots belonging to Ti and Pd structures, which form a common ring-like pattern in Fig. 2c. However, we can also observe disordered regions within the Ti and Pd grain interface (Fig. 3b), which can be

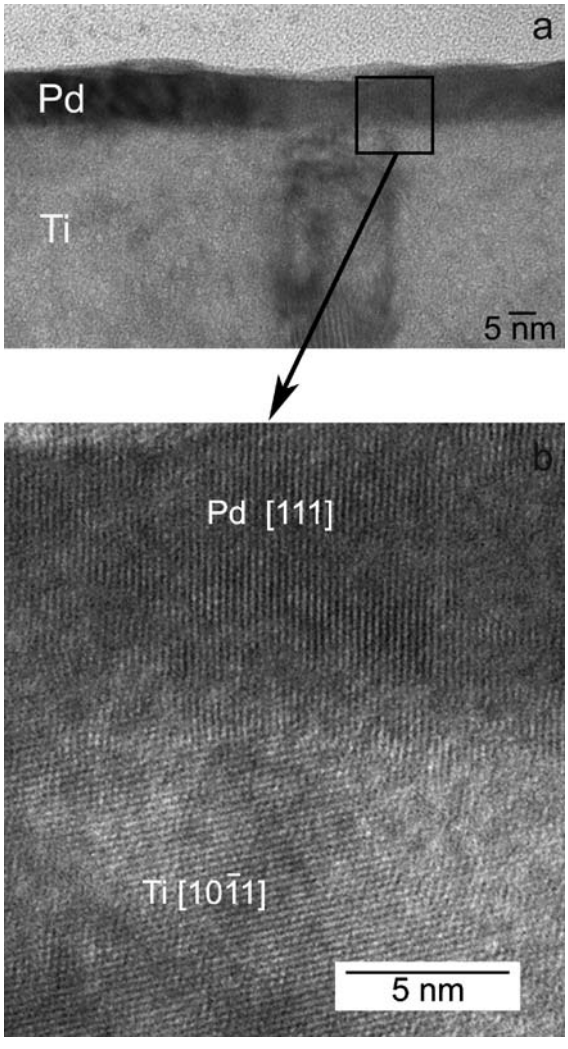


**Fig. 3** **a** Bright-field TEM image of the Pd/Ti film in cross-section at high-magnification. **b** Enlargement of the *square selected area in a* illustrating structural relationships between Pd and Ti grains within the interface region

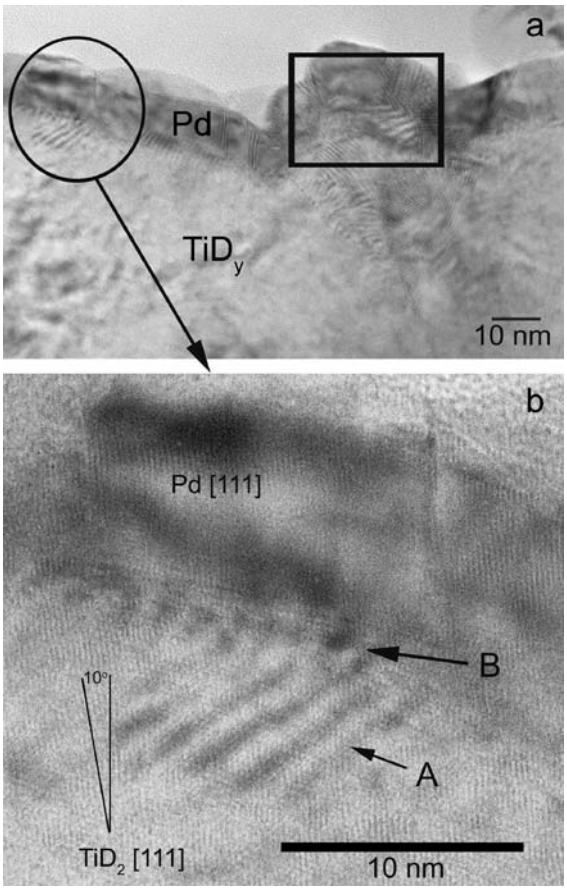


**Fig. 4** **a** Bright-field TEM image of the Pd/$TiD_y$ film in cross-section at high-magnification. **b** Enlargement of the *circular selected area in a* illustrating structural relationships between Pd and $TiD_y$ grains within the interface region. Moiré fringes (*A*) reveal the overlap of two $TiD_2$(111) lattices rotated through 10°. Moiré superstructure (*B*) is produced by overlapping $TiD_2$(111) and Pd (111) lattices

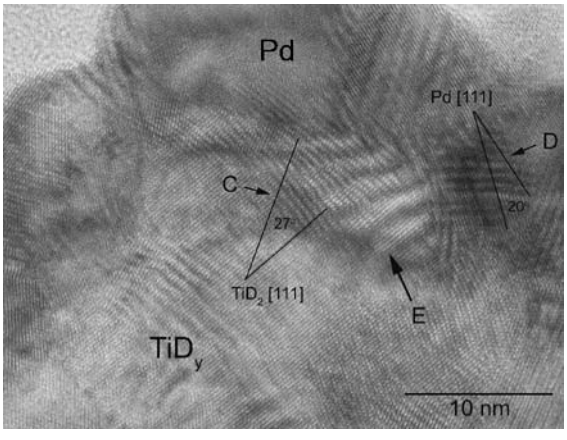


**Fig. 5** Enlargement of the *rectangular selected area* in the TEM image of the Pd/$TiD_y$ film in cross-section (Fig. 4a) illustrating complex structural relationships between Pd and $TiD_y$ grains within the interface region. Moiré fringes (*C*) appear as a result of overlapping of two $TiD_2$(111) lattices rotated through 27°. Moiré superstructure (*D*) is produced by the overlap of two Pd(111) lattices rotated through 20°. Complex Moiré fringes (*E*) are formed by the overlap of structure (*C*) with $TiD_2$(111) and Pd(111) lattices

ascribed to the formation of an intermediate amorphous phase. The amorphisation of the Pd/Ti films during deposition and annealing has been discussed in detail elsewhere [22]. The authors present experimental and thermodynamic evidence for the formation of amorphous structures in the interface region of the Pd/Ti multilayer films, sputter-deposited at both room and elevated temperature [22]. We also observe similar amorphous structures in the interface region of the evaporated Pd/Ti bi-layer. This structure is formed most likely during the initial stage of the Pd deposition by Pd vapour particles interacting with the Ti film surface.

Distinct structure variations can be observed within the Pd/$TiD_y$ interface region (Fig. 4a). Figure 4a shows strong evidence supporting the idea that the $TiD_y$ layer is plastically deformed, and causing the roughness of the overlapping thin Pd layer to increase. The plastic deformation of the $TiD_y$ film is a consequence of complex reactions leading to $TiD_y$ formation. According to Smithson et al. [6] the energy of this process is a superposition of two large effects: (1) expansion of the Ti metal structure into the lattice parameter of the hydride (deuteride), and (2) chemical bonding of hydrogen (deuterium) leading to $TiD_y$ formation. Evidence for the susceptibility to plastic deformation of titanium hydride material has recently been found experimentally [23].

Enlargements of high-magnification zoomed-in TEM images (Figs. 4b and 5) reveal a complex structure of the Pd/$TiD_y$ film interface. One can distinguish Moiré patterns as a result of the interference between various structures of adjacent Pd and $TiD_y$ grains within the interface region. The origin of these structures can be determined using well-known formulae describing translational and rotational Moiré fringes [24].

The translational Moiré fringe spacing $d_T$ is given by the expression:

$$d_T = \frac{d_1 d_2}{d_1 - d_2} \tag{1}$$

where $d_1$ and $d_2$ are the overlapped crystal lattice spacing of two various but parallel crystal planes.

The rotational Moiré fringe spacing can be evaluated from the relationship:

$$d_R = \frac{d}{2 \sin \beta/2} \tag{2}$$

where $d$ is a crystal lattice space of two identical superimposed crystal planes rotated through an angle $\beta$.

Selected areas within the TEM images of Figs. 4b and 5, representing various Moiré patterns, were examined using Eqs. 1 and 2 and experimental crystal lattice spacing data from the International tables for X-ray crystallography ICDD-JCPDS data base [21]. The results are summarized in Table 1. The evaluated Moiré fringe spacings were in agreement with those as measured from the lattice fringes of the TEM images in Figs. 4b and 5. By observing Figs. 4b and 5 it should be noted that the Moiré superstructures within the Pd/$TiD_y$ interface region were found to originate from interference of lattice planes within both the $TiD_y$ (spots A, C) and Pd (spot D) phases as well as from overlapping of lattice planes of adjacent Pd and $TiD_y$ grains (spots B, E).

The variety of complex Moiré fringes within the Pd/$TiD_y$ interface region indicates a disordered character. Both stress-induced deformation of the $TiD_y$ layer accompanying the Ti lattice expansion during $TiD_y$ formation and post-evaporation of the Pd film could explain this distortion. In the latter process part of the deuterium can be released from the $TiD_y$ layer by thermally excited Pd particles at the initial stage of Pd film growth, causing a structural orientation of interacting $TiD_y$ grains to be disturbed.

## XPS analysis of Pd/$TiH_y$ interface region

The chemical nature of the components formed within the interface region of the Pd/$TiD_y$ film was investigated by means of XPS. To enable such an analysis, the thickness of the Pd top layer should be less than the effective probing depth of XPS (ca. 3 nm [25]). The 12-nm-thick Pd layer, covering the $TiD_y$ film, therefore prevents an effective XPS

**Table 1** Examination of selected Moiré patterns on the cross-sectional TEM images of the Pd/$TiD_y$ film in Figs. 4 and 5

| Spot | Moiré fringe spacing (nm) | | | Overlapped lattice planes |
|---|---|---|---|---|
| | As measured[a] | Evaluated | | |
| | | $d_T$ | $d_R$ | |
| A (Fig. 4b) | 1.47±0.06 | | 1.48 | $TiD_2$ (111) rotated through 10° |
| B (Fig. 4b) | 1.69±0.14 | 1.73 | | $TiD_2$ (111) and Pd (111) |
| C (Fig. 5) | 0.54±0.02 | | 0.55 | $TiD_2$ (111) rotated through 27° |
| D (Fig. 5) | 0.66±0.02 | | 0.65 | Pd (111) rotated through 20° |
| E (Fig. 5) | 1.74±0.10 | 1.73 | | $TiD_2$ (111) and Pd (111) |

[a]The "as measured" Moiré fringe spacing is compared with the spacing evaluated using Eqs. 1 and 2

analysis of the Pd/$TiD_y$ interface. In order to allow for a meaningful analysis of this interface, the film was etched continuously with $Ar^+$ ions until the Ti 2p XPS peaks appeared. Figure 6 shows the XPS survey spectra obtained for the same sample before (spectrum 1) and after removing approximately 11 nm of the Pd top layer (spectrum 2). The presence of Ti peaks, in addition to those associated with Pd, can be clearly observed in spectrum 2.

Figure 7 shows a set of detail spectra recorded after the $Ar^+$ sputtering procedure described above for Pd/$TiD_y$ (lines 1). These spectra are compared with the corresponding spectra collected on separate $TiD_y$ (lines 2), Ti (lines 3) and Pd (lines 4) films, respectively, after they were $Ar^+$-etched for the same time as for the Pd/$TiD_y$ sample. By presenting the spectra in this way, a BE shift of Ti and Pd XPS spectra, as a result from deuterium and oxygen interaction, can be assigned more accurately. The Ti 2p spectra (Fig. 7a) of the Pd/$TiH_y$ and $TiD_y$ films (lines 1 and 2, respectively) are characterised by the Ti $2p_{3/2}$ peak at BE=454.6 eV, which is shifted 0.6 eV towards higher binding energy as compared to the Ti 2p spectrum of the Ti film (line 3). The shift of the Ti 2p peak with respect to the corresponding pure Ti agrees well with our findings for $TiH_y$ and Au/$TiH_y$ films [7, 12] and with the data reported by other authors for titanium hydride materials (0.5–0.7 eV

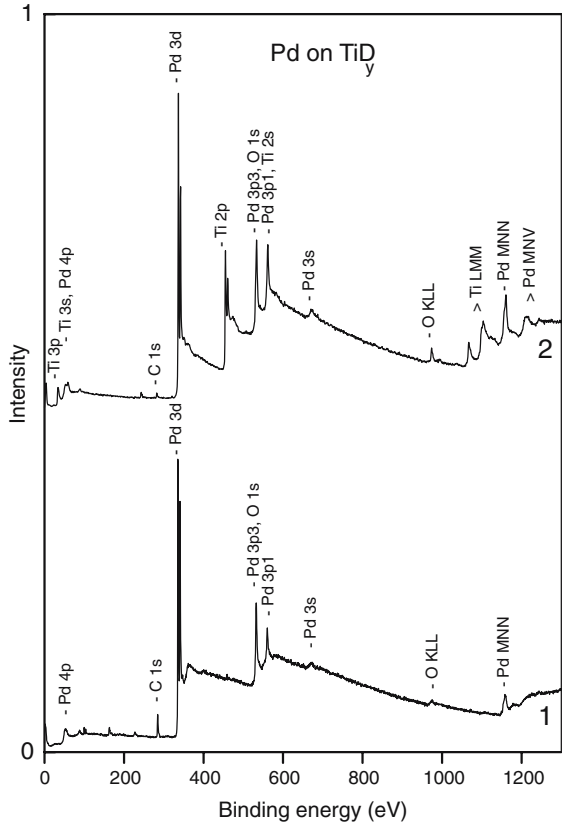


**Fig. 6** Wide XPS binding energy spectra of the Pd/$TiD_y$ film before (*line 1*) and after removing approximately11 nm of the Pd top layer by Argon ion sputtering (*line 2*). From the cross-sectional TEM image (see e.g. Fig. 2b) the thickness of the Pd top layer before $Ar^+$ etching was determined to be 12–13 nm

[26–28]). The XPS peak at BE approximately 458.0 eV (marked by the arrow in Fig. 7a) indicates a trace contamination of titanium oxide compounds. However, since a large scatter in BEs was reported for various titanium oxides [19], an assignment of this peak to a specific chemical species is not possible. Moreover, the observed peak can also be associated with TiOD [7, 29] which could be formed within the Pd/$TiD_y$ interface due to oxygen interaction with the $TiD_y$ phase.

The tungsten heater used for Pd film evaporation is most likely the source of a small concentration of oxygen within the Pd/$TiD_y$ region, since this heater cannot be completely out-gassed before Pd film deposition. This is due to a relatively low temperature of evaporation [30]. Therefore, the release of a small amount of oxygen from a tungsten heater during the Pd film evaporation is unavoidable causing both $TiD_y$ (Ti) and Pd interface layers to be contaminated.

Evidence for oxygen interaction with the Pd layer is provided by the Pd 3d XPS spectra presented in Fig. 7b. Spectrum 1, taken from the Pd/$TiD_y$ interface, is shifted towards higher BE as compared to the corresponding spectrum of the pure Pd film (line 4). The Pd $3d_{5/2}$ peak position at BE=336.5 eV corresponds well with the XPS data reported for palladium oxide [31, 32, and other refs. in 19].

Normally, an analysis of the O 1s XPS spectrum is useful and yields complementary information in the interpretation of metal oxide states. However, in the case of Pd compounds this procedure is complicated by the overlap of the O 1s and Pd $3p_{3/2}$ states. Figure 7c shows the spectra recorded on the Pd/$TiD_y$ (line 1), $TiD_y$ (line 2) and pure Pd (line 4) films. The last one exhibits a pure Pd $3p_{3/2}$ XPS state, which expands within the entire BE region of the O 1s peak, making the interpretation of overlapping oxygen states rather ambiguous. Nevertheless, we can observe two distinct peak areas forming the XPS spectrum recorded at the Pd/$TiD_y$ interface (line 1). First, the peak at about 531.0 eV BE can be assigned to Ti oxides [12, 19, 33] which is similar to the features associated with the $TiD_y$ film (line 2) in the O 1s spectrum. The second one at approximately 533.4 eV BE is dominated by a strong contribution of the Pd $3p_{3/2}$ state, a peak coinciding with the O 1s state of OH and $H_2O$ [7, 19, 34–36].

The valence band (VB) spectra (Fig. 7d) recorded on Pd/$TiH_y$ (line 1), $TiD_y$ (line 2), Ti (line 3) and Pd (line 4) layers reveal a complex character of the VB spectrum in the interface of the Pd/$TiH_y$ specimen. This spectrum is dominated by Pd valence band components. The main peak at 3.8 eV (line 1) is similar to that found on the Pd film (line 4) but slightly narrower and shifted about 2.5 eV towards higher BE, the higher-energy part of this spectrum is significantly lower than the corresponding part of the Pd spectrum. Low-intensity states between 2 and 12 eV, characteristic for titanium hydrides [6, 26, 28] (see line 2), are screened by the high-energy part of this spectrum. However, the $TiD_y$ phase that coexists with Pd in the Pd/$TiH_y$ interface, causes the intensity of the VB spectrum in this BE region to be lower than that of Pd. On the other

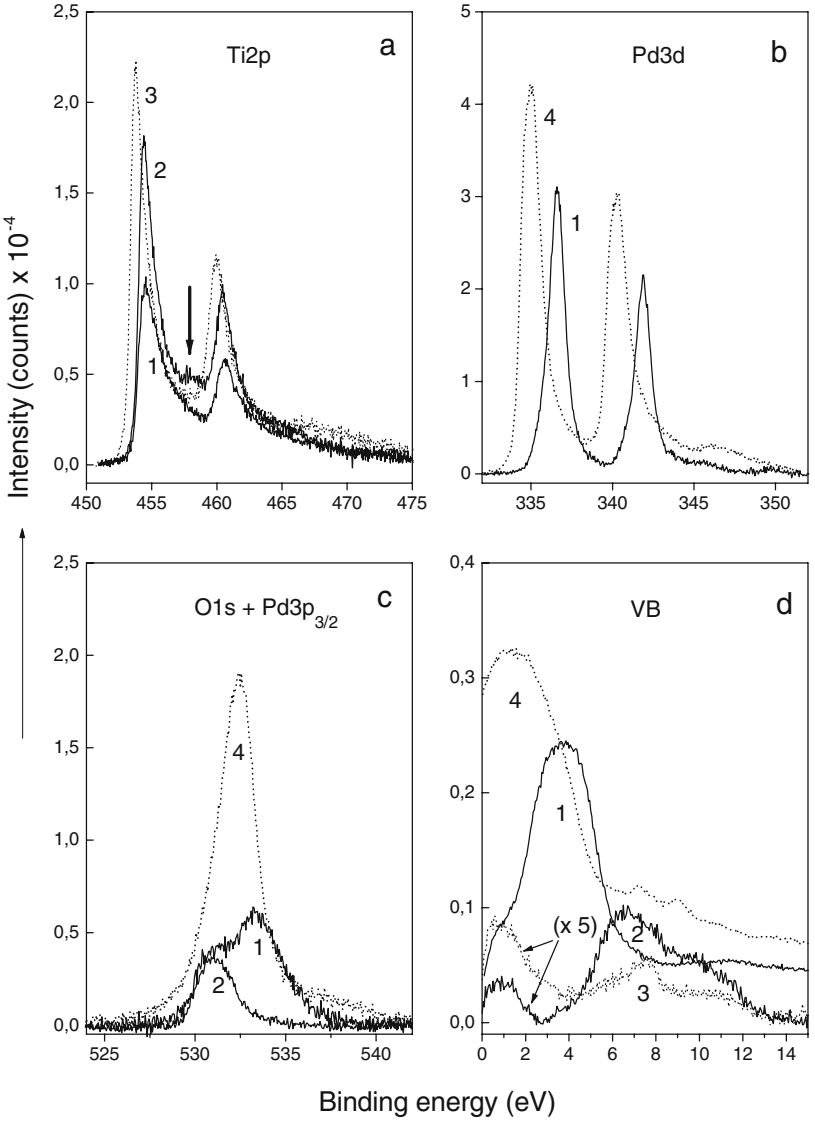


**Fig. 7** Ti 2p (**a**), Pd 3d (**b**), O 1s + Pd $3p_{3/2}$ (**c**) and valence band (VB) (**d**) XPS spectra of the Pd/$TiD_y$ (*lines 1*), $TiD_y$ (*lines 2*), Ti (*lines 3*) and Pd (*line 4*) films after a short $Ar^+$ sputtering time. The *arrow* in (**a**) indicates the Ti 2p state of titanium oxide (see text). The intensity scale of *lines 2* and *3* in (**d**) is expanded by a factor of 5

hand, the intensity of the band just below Fermi level at approximately 0.7 eV, appears relatively strong as compared to that of $TiD_y$ and pure Ti (see lines 2 and 3, respectively). It is interesting to note that similar features in the VB spectra were reported for $Pd_3Ti$ and $PdTi_2$ alloys [37]. In these studies the relative increase of the lowest BE component in the $PdTi_2$ VB spectrum was explained as a result of an increase in d-character at the Ti site at the Fermi level due to Pd–Ti d–d interactions. For the $PdTiD_y$ interface this phenomenon is even more pronounced indicating an almost tenfold increase of this VB band intensity relative to the corresponding band of $TiD_y$ (compare lines 1and 2 in (d)).

## Conclusions

A 10- to 12-nm-thick film of Pd, evaporated in situ onto the $TiD_y$ layer forms a good protection of the titanium hydride material against air interaction. The protecting Pd layer exhibits a fine-grained surface morphology. High-magnification cross-sectional TEM images reveal the $TiD_y$ film to be plastically deformed, resulting in an increase in roughness of the top Pd layer. The chemical nature of $TiD_y$ was identified in the Ti 2p XPS spectrum by a Ti $2p_{3/2}$ peak shape shifted with 0.6 eV BE relative to the corresponding pure Ti. Complex structures, including Moiré patterns, have been identified within the Pd/$TiD_y$ interface. Besides $TiD_y$ and Pd, TiO and PdO were detected by XPS to be the main chemical compounds in the interface region of the Pd/$TiD_y$ film. The electronic structure of the Pd/$TiD_y$ interface, as revealed by the XPS VB spectrum, exhibits Pd–Ti bimetallic-type features.

## References


1. Westlake DG, Satterthwaite CB, Weaver JH (1978) Physics Today 31:32–39
2. Hirooka Y (1984) J Vac Sci Technol A 2:16–21
3. Kirchheim R, Fromm E, Wicke E (1989) (eds) Metal-hydrogen systems: Fundamentals and applications (Proceedings of the first international symposium combining "hydrogen in metals" and "metal hydrides" Stuttgart, 1988), R Oldenburg Verlag
4. Conforto E, Caillard D, Aronsson BO, Descouts P (2004) Phil Mag 1:631–645
5. Nowicka E, Wolfram Z, Lisowski W, Duś R (1996) Appl Surf Sci 93:53–58
6. Smithson H, Marianetti CA, Morgan D, Van der Ven A, Predith A, Ceder G (2002) Phys Rev B 66:144107(1–10)
7. Lisowski W, van den Berg AHJ, Smithers M (1998) Surf Interface Anal 26:213–219
8. Heller EMB, Suyver JF, Vredenberg AM, Boerma DO (1999) Appl Surf Sci 150:227–234
9. Checchetto R, Bazzanella N, Miotello A, Principi G (2003) J Alloys Compd 356–357:521–525
10. Kulkova SE, Eremeev SV, Egorushkin VE, Kim JS, Oh SY (2003) Solid State Com 126:405–408
11. Kim JS, Oh SY, Lee G, Koo YM, Kulkova SE, Egorushkin (2004) Int J Hydrogen Energy 29:87–92
12. Lisowski W, van den Berg AHJ, Leonard D, Mathieu HJ (2000) Surf Interface Anal 29:292–297
13. Lisowski W (1999) Vacuum 54:13–18
14. Duś R, Lisowski W, Nowicka E, Wolfram Z (1995) Surf Sci 322:285–292
15. Lisowski W, Keim EG, Smithers M (2002) Appl Surf Sci 189:148 –156
16. Anthony MT (1983) In: Briggs D Seah MP (eds) Practical surface analysis by Auger and X-ray photoelectron spectroscopy. Wiley, Chichester, Apendix 1, p 431
17. Ikeo N, Jijima Y, Niimura N, Sigematsu M, Tazawa T, Matsumoto S, Kojima K, Nagasawa Y (1991) Handbook of X-ray photoelectron spectroscopy. JEOL, USA
18. Seah MP (1999) Appl Surf Sci 144–145:161–167
19. Wagner CD, Naumkin AV, Kraut-Vass A, Allison JW, Powell CJ, Rumble JR Jr (2003) NIST Standard Reference Database 20, Version 3.4, Web Version: http://www.srdata.nist.gov/xps/
20. Jouneau PH, Stadelmann P, EMS on line, http://www.cimesg1.epfl.ch/CIOLS
21. International tables for x-ray crystallography ICDD-JCPDS data base; Pd: card 00-046-1043, Ti: card 00-044-1294, $TiH_{1.971}$: card 00-007-0370
22. Tadayyon SM, Fujimoto Y, Tanaka K, Doi M, Matsui M (1994) Jpn J Appl Phys 33:4697–4702
23. Chen CQ, Li SX, Zheng H, Wang LB, Lu K (2004) Acta Mater 52:3697–3706
24. Williams BD, Carter CB (1996) Transmission electron microscopy. Plenum, New York, chap 27
25. Feldman LC, Mayer JW (1986) Fundamentals of surface and thin film analysis. Elsevier, The Netherlands, chap 9 and p 352
26. Lamartine BC, Haas TW, Solomon JS (1980) Appl Surf Sci 4:537–555
27. Riesterer T (1987) Z Phys B Condens Matter 66:441–458
28. Weaver JH, Peterman DJ, Peterson DT, Franciosi A (1981) Phys Rev B 23:1692–1698
29. Sham TK, Lazarus MS (1979) Chem Phys Lett 68:426–432
30. Honig RE (1962) RCA Rev 23:567–586
31. Tressaud A, Khairoun S, Touhara H, Watanabe N (1986) Z Anorg Allg Chem 540:291–299
32. Moddeman WE, Bowling WC, Carter DC, Grove DR (1988) Surf Interface Anal 11:317–326
33. Rao CNR, Sarma DD, Vasudevan S, Hegde MS (1979) Proc R Soc London A 367:239–252
34. Lausmaa J, Kasemo B, Mattsson H (1990) Appl Surf Sci 44:133–146
35. Kerber SJ, Brucker JJ, Wozniak K, Seal S, Hardcastle S, Barr TL (1996) J Vac Sci Technol A 14:1314–1320
36. McCafferty E, Wightman JP (1999) Appl Surf Sci 143:92–100
37. Bzowski A, Sham TK (1993) Phys Rev B 48:7836–7840